Defect-Complex Engineering to Improve the Optoelectronic Properties of $CuInS_2$ by Phosphorus Incorporation

Huiwen Xiang,[1,2] Jinping Zhang,[2] Feifei Ren,[1] Rui Zhu,[1] Yu Jia,[1] and Chengyan Liu[1,2,*]

[1] *Key Laboratory for Special Functional Materials of Ministry of Education, Henan Key Laboratory of Photovoltaic Materials, and School of Materials Science and Engineering, Henan University, Kaifeng 475004, China*

[2] *Faculty of Engineering, Huanghe Science and Technology College, Zhengzhou 450006, China*

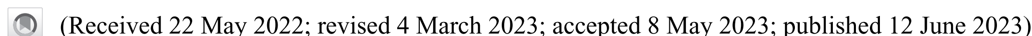

(Received 22 May 2022; revised 4 March 2023; accepted 8 May 2023; published 12 June 2023)

Pure disulfide $CuInS_2$ (CIS) with a proper band gap (∼1.53 eV) is a promising photovoltaic material, yet it exhibits a relatively low power-conversion efficiency among the Cu-III-VI_2 (III = In, Ga; VI = S, Se) chalcopyrite solar cells. First-principles calculations show that the inferior photovoltaic performance of CIS solar cells can be attributed to several factors, including a strong compensation effect, great band-tail states, and defect levels within the band gap, which result in a limited carrier concentration and severe nonradiative recombination of carriers. The strong compensation effect between the In_{Cu} donor and Cu_{In} or V_{Cu} acceptor defects makes it difficult to maintain a desired p-type conductivity as the elemental chemical potential changes. Besides, In_{Cu}- and Cu_{In}-related defects induce a downward shift of the conduction-band minimum and an upward shift of the valence-band maximum, respectively. The presence of the Cu_{In}-defect level within the band gap is inevitable under the In-poor and S-rich conditions required for the p-type characteristic of CIS. To address these issues, we find that phosphorus (P) incorporation, forming an isoelectronic $2P_S + In_{Cu}$ defect complex, can enhance the p-type characteristic by consuming the residual electrons of In_{Cu}-donor defects and alleviate their band-tail states by introducing substantial atomic orbital coupling of P_S and In_{Cu} defects. Moreover, the required In-rich, S-poor, and P-rich conditions, to facilitate the formation of the beneficial $2P_S + In_{Cu}$ defect complex, can also suppress the formation of Cu_{In} defects, accordingly, reducing the associated band-tail state and defect state. This study reveals the origins of the stagnated efficiency of CIS and that defect-complex engineering by anion doping is a feasible way to improve the electronic properties of multicomponent semiconductors.

DOI: 10.1103/PhysRevApplied.19.064036

I. INTRODUCTION

Chalcopyrite Cu-III-VI_2 (III = In, Ga; VI = S, Se) semiconductors are considered leading candidates of highly efficient photovoltaic materials due to their great off-stoichiometric tolerance, tunable electrical conductivity, and excellent optoelectronic properties. Among them, pure disulfide $CuInS_2$ (CIS) is a promising photovoltaic material, owing to its optimal direct band gap (∼1.53 eV) and nontoxic constituents. However, its record power-conversion efficiency is stagnated at 11.4% [1], much lower than 15.5% for $Cu(In, Ga)S_2$ (CIGS) [2], 19.2% for $CuInSe_2$ (CISe) [3], and 23.4% for $Cu(In, Ga)(S, Se)_2$ (CIGSSe) [4]. The considerable efficiency gap between CIS and the other chalcopyrite solar cells should be attributed to the large deficit of open-circuit voltage (V_{OC} deficit), which is defined as $E_g/q - V_{OC}$, where E_g is the band gap, V_{OC} is the open-circuit voltage, and q is the electron charge. The champion CIS solar cell has a V_{OC} deficit of about 800 mV [1], whereas disulfide CIGS and diselenides (CISe and CIGSSe) have deficits of about 630 mV [2] and less than 400 mV [3,4], respectively, as listed in Table S1 within the Supplemental Material [5].

Generally, the great loss of V_{OC} in solar cells mainly stems from the severe photogenerated-carrier nonradiative recombination caused by the defective bulk and an unfavorable interface [6]. It is experimentally proven that the dominant recombination mechanism in chalcopyrite solar cells depends on the Cu stoichiometry in the absorber layer [7–12]. Specifically, Cu-rich [Cu:(In,Ga) > 1] devices usually suffer from severe carrier recombination at the interface between absorber and buffer layers, caused by the defective interface, as a consequence of the mandatory etching process, while Cu-poor [Cu:(In,Ga) < 1] ones do not [11–16]. Regardless of the sulfide or selenide chalcopyrite, most of the record efficiencies of chalcopyrite solar cells are achieved using a Cu-poor absorber [2–4]. But even under Cu-poor conditions that are free of

*cyliu@henu.edu.cn

 © 2023 American Physical Society

etching, the V_{OC} deficit of the most-efficient pure-sulfide chalcopyrite solar cell is still larger than 600 mV [2]. From crystallographic analysis, the inferior performances of sulfide chalcopyrite solar cells compared with selenide ones are attributed to lower structural stability of the former under Cu-poor conditions [17]. However, this is only applicable to a considerably Cu-poor case, since experiments show that sulfide absorbers with a Cu:(In + Ga) ratio of around 0.9 are well indexed to a good chalcopyrite crystal structure [12]. To locate the cause of the large V_{OC} deficit in CIS devices, the properties of the absorber layer are separated from the effects of the interface. It is then identified that the quasi-Fermi-level splitting, which indicates the upper limit of V_{OC}, is enhanced by reducing the deep-level defects in the bulk [10]. To date, a detailed understanding of the intrinsic defects in CIS is still lacking. Theoretically, a previous study claimed that In_{Cu}, Cu_{In}, and V_{In} defects had serious deep levels [18], while the calculated negative formation energies of these charge-neutral defects violated the endothermic reaction for generating defects in a perfect bulk; hence, the conclusion regarding the deep-level defects of CIS needs to be revisited. Recent calculations indicated that donor defects of Cu_i and In_{Cu} and acceptor defects of V_{Cu} and Cu_{In} were dominant in CIS, among which the Cu_{In} defect had a defect state within the band gap [19]; this is consistent with a more recent report that identified antisite Cu_{In} and Cu_{Ga} defects as the major performance-limiting deep-level defects in CIGS [12]. As the experimental results show, by using a Cu-poor absorber, the interface and bulk recombination can be reduced through free etching and suppression of the Cu_{In} and Cu_{Ga} defects, respectively. Nevertheless, it is notable that the Cu-poor absorber has a much lower carrier concentration of 10^{15} cm^{-3} relative to its Cu-rich counterpart [12]. Additionally, experiments provide clues that band-tail states caused by defects in CIS increase carrier recombination, although the specific defects are not identified [20]. Therefore, proposing a feasible scheme to reduce possible nonradiative recombination of carriers and produce a high carrier concentration is urgently needed and of great importance for highly efficient CIS. Our recent work found that the incorporation of anions to form a defect complex consisting of anion and cation point defects could effectively eliminate severe deep levels and band-tail states caused by intrinsic defects. This is achieved through substantial atomic orbital coupling, which is successfully applied in the passivation of Sn_{Zn} defects by forming a $2P_S + Sn_{Zn}$ defect complex via phosphorus (P) doping in $Cu_2ZnSnS(e)_4$ [21]. Previous experimental and theoretical studies also revealed that P doping could effectively reduce V_{OC} loss in CdTe [22] and enhance the p-type conductivity of CIS [23,24]. These findings indicate that defect engineering through P doping could be a promising way to improve the photovoltaic performance of chalcogenide semiconductors.

Here, we reveal the causes for the low efficiency of CIS in terms of defects in the bulk and present the benign effects of P anion incorporation. By performing first-principles calculations, we find that the p-type strength of CIS is limited by the compensation of intrinsic defects, serious band-tail states are introduced by In_{Cu}- and Cu_{In}-related defects, and defect levels within the band gap are inevitable due to the Cu_{In}-related defects promoted by the In-poor conditions required for the desired p-type characteristic. These defects should be responsible for severe nonradiative recombination of carriers in the bulk, and thus, the considerable loss of V_{OC} in the CIS solar cell. Furthermore, we find that P incorporation to form the isoelectronic $2P_S + In_{Cu}$ defect complex not only enhances the p-type strength by consuming the residual electrons of the In_{Cu}-donor defect but can also heal the band-tail states by introducing strong atomic orbital coupling. Moreover, the In-rich, S-poor, and P-rich conditions required to promote the formation of the beneficial $2P_S + In_{Cu}$ defect complex suppress the formation of the Cu_{In} defect with a defect level within the band gap and can reduce interfacial recombination by avoiding the etching process during experimental fabrication. The small region of the phase diagram for effective P incorporation into CIS suggests that the synthesis conditions should be carefully controlled to avoid the formation of undesired secondary phases.

II. CALCULATION METHOD

The total energies and electronic structures of various defect systems, as well as the defect-free bulk, are calculated based on a $2 \times 2 \times 1$ cubic supercell containing 64 atoms. First-principles calculations are implemented in the Vienna *ab initio* simulation package [25,26] with the standard frozen-core projector-augmented-wave method [27]. The Perdew-Burke-Ernzerhof (PBE) exchange-correlation functional is employed to relax structures [28]. All of the formation energies and band structures are calculated by static calculations with the Heyd-Scurseria-Ernzerhof-06 (HSE06) hybrid exchange-correlation functional [29] based on PBE-relaxed atomic structures. A mixing parameter of 0.36 is used to correct the band gap of CIS to the experimental value (about 1.53 eV) [30]. The cutoff energy for basis functions is 400 eV, and the k points are sampled with a $3 \times 3 \times 3$ mesh in the Brillouin zone with the Γ point [31]. Defect models are fully relaxed with Hellmann-Feynman forces less than 0.01 eV/Å and electronic convergence less than 1×10^{-4} eV. Additionally, we examine larger $3 \times 3 \times 1$ and $3 \times 3 \times 2$ supercells to calculate the band structures and formation energies of the two dominant defects, which give similar results to the $2 \times 2 \times 1$ supercell (see Part III of the Supplemental Material [5]).

III. RESULTS AND DISCUSSION

A. Band alignment

Usually, absorbers of highly efficient chalcopyrite single-junction cells are designed to be p type [2–4], despite the bipolar-conductivity ability of CIS and CISe via stoichiometric control [32–34]. One practical reason is that n-type transparent conducting layers are more available than the p-type ones at present. In addition, for conventional photovoltaic materials, electrons, as minority carriers with a small effective mass in a p-type absorber, are more easily extracted than holes, as minority carriers with a large effective mass in an n-type absorber. The theoretically calculated band-edge energetics of several chalcopyrite absorbers and the commonly used buffer layer CdS, as shown in Fig. 1, are convenient to judge whether the extraction of electrons and the p-type conductivity of the absorber can be promoted. It is evident that CIS not only has an optimal band gap to match the solar spectrum [40] but also shows a favorable spikelike conduction-band offset (CBO) with CdS, which is supported by photoelectron spectroscopy measurements [41]. It is notable that several studies observe different amplitudes of clifflike CBOs in CIS/CdS interfaces [42–44], caused by different interfacial chemistries that are significantly dependent on the preparation process [45,46]. By comparison, despite the suitable CBO, CISe has a small band gap, and In-free $CuGaS_2$ and $CuGaSe_2$ have oversized band gaps as well as unfavorable clifflike band offsets. Although partly substituting In with Ga can increase the band gap of CISe, unmanageable Ga diffusion can lead to alloy disorder and unfavorable band alignment at the CIGSe/CdS interface [47–49]. Therefore, among these chalcopyrite absorbers, CIS is superior in terms of optical band gap, band offset, and absorber homogenization. However, according to the doping-limit rule [39,50], the lower valence-band maximum (VBM) of CIS than the Fermi-energy-pinning level for p-type doping (see Fig. 1) suggests that the p-type strength of CIS is likely to be restrained by factors such as the significant compensation effects of donor and acceptor defects, which limit a further shift of the Fermi level. In principle, CIS is promising for showing an excellent photovoltaic performance if the sufficient p-type conductivity is maintained and harmful defects are improved simultaneously.

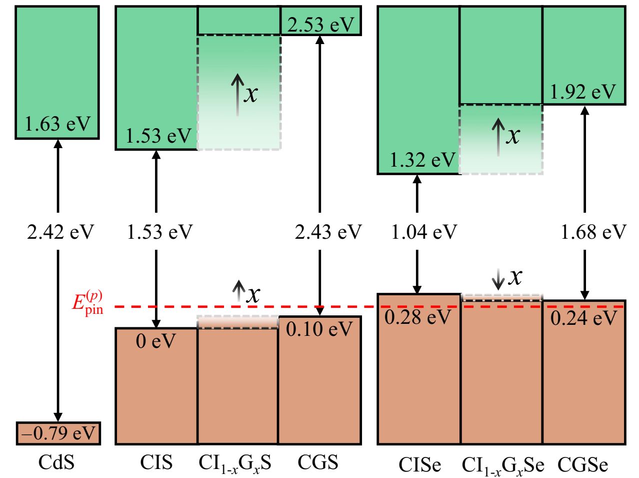

FIG. 1. Comparison of band-edge energetics among CdS, CIS, $CuIn_{1-x}Ga_xS_2$ ($CI_{1-x}G_xS$), $CuGaS_2$ (CGS), CISe, $CuIn_{1-x}Ga_xSe_2$ ($CI_{1-x}G_xSe$), and $CuGaSe_2$ (CGSe) by collecting values from Refs. [35,36]. Values of the band gap are obtained from experimental measurements [37]. Gradual arrow denotes the direction to which the band edge changes as x increases. Red dashed line represents the Fermi-energy-pinning level for p-type doping [38]. VBM far below the red line indicates the difficulty of p-type doping based on the doping-limit rule [39].

B. Phase diagram and defect-formation energies

Our recently proposed passivation strategy for deep-level defects indicated that the anion substitutional defect associated with harmful cation antisite defects could form a benign isoelectronic defect complex, which played a significant role in eliminating deep levels and alleviating band-tail states [21]. A previous experiment found that InP incorporation could make CIS a desired p-type conductivity under S-poor conditions [23], which usually result in an n-type conductivity of chalcopyrite. These indicate that anion P doping is well worth trying to improve the defect properties and electrical conductivity of CIS by forming an isoelectronic defect complex composed of P_S acceptor defects and antisite donor defects, such as the $2P_S + In_{Cu}$ defect complex.

The electrical conductivity, transition-energy levels of defects, and the effects of P incorporation in CIS are studied by calculating the defect-formation energy as a function of Fermi level and elemental chemical potential [51,52]. The available range of elemental chemical potentials of components is confined in the stable phase diagram of CIS with P incorporation, as shown in Fig. 2(a) (see the calculation details in Part II of the Supplemental Material [5]). The formation energy, $\Delta H(\alpha, q)$, of defect α in charge-state q can be expressed as [50,53]

$$\Delta H(\alpha,q) = \Delta E(\alpha,q) + \sum_i n_i\mu_i + qE_F, \tag{1}$$

$$\Delta E(\alpha,q) = E(\alpha,q) - E(\text{host}) + \sum_i n_i\mu_i^0 + qE_{\text{VBM}} - \varepsilon_{\text{ES}}, \tag{2}$$

where μ_i is the chemical potential of element i relative to that of its pure elemental phase, μ_i^0. E_F is the Fermi level referenced to the VBM of the CIS host represented by E_{VBM}. $E(\alpha,q)$ is the total energy of a fully relaxed

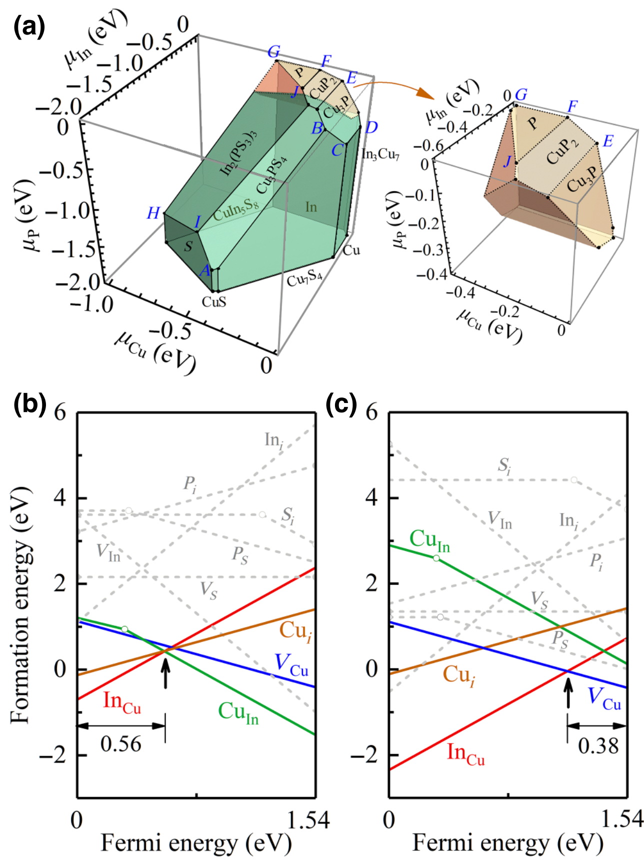

FIG. 2. Phase diagram and defect-formation energy as a function of Fermi energy. (a) Stable phase diagram of CIS depicted by the available range of elemental chemical potentials. Golden region represents the range of elemental chemical potentials with the enhanced p-type characteristic of CIS through effective P doping. Inset shows an enlarged local drawing of the golden region for clarity. (b),(c) Formation energies of defects as a function of Fermi level under chemical potential conditions of points A and G, respectively. Points A and G are labeled in (a), and the values of elemental chemical potential for the vertices in (a) are listed in Table S2 within the Supplemental Material [5]. Black one-way arrow labels the Fermi-energy-pinning level. Dashed and solid lines represent defects with relatively high and low formation energies, respectively.

supercell with defect α in charge-state q. E(host) is the total energy of a defect-free supercell, the size of which is the same as the defect system. n_i is the difference in atom numbers of element i between the defect system and the host. $n_i > 0$ as an atom is taken away from the host, while $n_i < 0$ as an atom is added to the host. ε_{ES} is the correction term for charged defects due to electrostatic interactions between periodic images in the used finite-size supercell, as determined by the SXDEFECTALIGN software [53–55].

The formation energies of point defects as functions of the Fermi level, as shown in Figs. 2(b) and 2(c), are studied under the chemical potential conditions represented by points A ($\mu_{Cu}=-0.47$ eV, $\mu_{In}=-1.63$ eV, $\mu_S=0$ eV, and $\mu_P=-1.69$ eV) and G ($\mu_{Cu}=-0.49$ eV, $\mu_{In}=0$ eV, $\mu_S=-0.81$ eV, and $\mu_P=0$ eV) in Fig. 2(a), which represent S-rich and S-poor conditions, respectively. The black one-way arrows in Figs. 2(b) and 2(c) indicate the Fermi-energy-pinning level, which is determined by the lowest crossing point of the lines for acceptor and donor defect-formation energies. It is seen that, under S-rich conditions (point A), CIS presents a weak p-type characteristic, as the Fermi-energy-pinning level, determined by competition between Cu_{In}^{2-} acceptor and In_{Cu}^{2+} donor defects, is located at 0.56 eV above the VBM. Under S-poor and In-rich conditions (point G), the Fermi level pinned by the V_{Cu}^{-} acceptor and In_{Cu}^{2+} donor defects is located at 0.38 eV below the conduction-band minimum (CBM), indicating a relatively strong n-type characteristic of CIS. The dependence of electrical conductivity on the synthesis conditions in CIS is consistent with previous experimental and theoretical results [18,19,33,56]. Although the S-rich conditions result in the desired p-type characteristic of CIS, the accompanying In-poor conditions facilitate the formation of Cu_{In} defects with a transition-energy level at 0.31 eV above the VBM, as shown in Fig. 2(b). The defect level within the band gap, which can act as a nonradiative recombination of carriers center is one of the factors limiting the photovoltaic efficiency of solar cells. In contrast, under the S-poor conditions, the formation of Cu_{In} acceptor defects can be effectively limited due to their high formation energy [see Fig. 2(c)], but the undesired n-type characteristic of CIS is promoted by the energetically favorable In_{Cu}^{2+} donor defects. Moreover, the In_{Cu} defects induce considerable band-edge fluctuation, as discussed in the next section. Considering P incorporation, the introduced P_i and P_S point defects have high formation energies, even under the most P-rich conditions, which have little adverse impact on the electrical properties of CIS. The influences of the P-containing defect complexes are discussed in Sec. III D.

C. Components of band structures

Understanding the electronic structure of a semiconductor is essential to optimize the electrical properties of defects. Figure 3(a) presents the band structure of defect-free CIS weighted by atomic orbitals, and it is seen that the conduction-band edge is very dispersive, while the valence-band edge is relatively localized. The projected density of states combined with the schematic diagram of atomic orbital coupling in Fig. 3(b) illustrate that the VBM of CIS is dominated by the antibonding state of Cu $3d$-t_{2g}/S $3p$ orbitals, as previously evidenced by theoretical studies [18,19,57]. The fully occupied antibonding state tends to weaken the Cu-S bond, promoting the formation of V_{Cu} defects in CIS [32]. Moreover, the V_{Cu} defects leave a dangling-bond state, which originates from the unsaturated S $3p$ orbital inside the valence band. This is consistent with

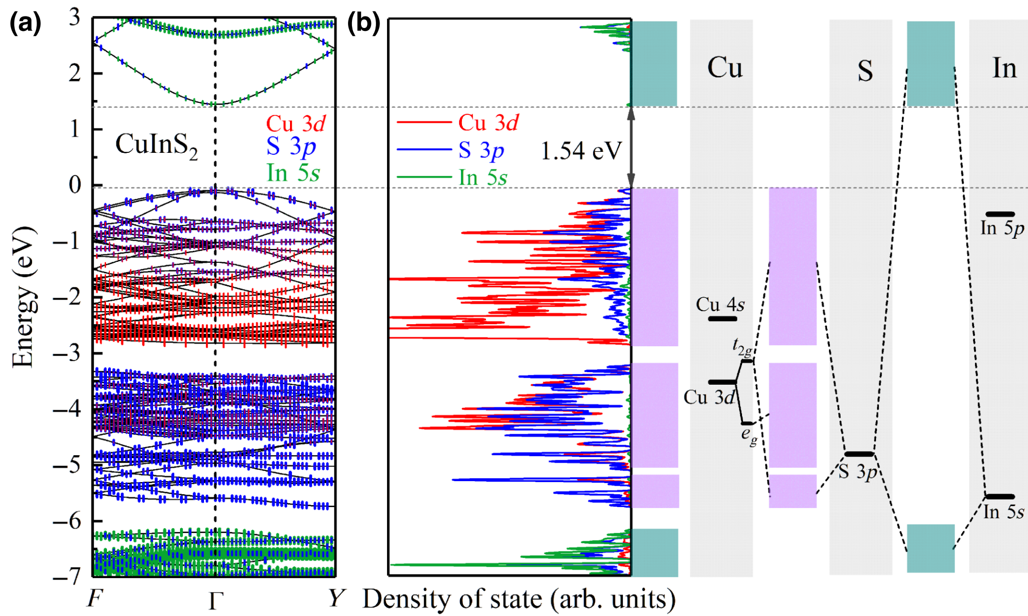

FIG. 3. Band-structure components of pristine CIS. (a) Band structure of pristine CIS weighted by atomic orbitals. (b) Band-edge components analyzed from the projected density of states and presented using a schematic diagram of atomic orbital coupling. VBM is dominated by the antibonding state of Cu $3d$-t_{2g}/S $3p$ orbital coupling, while the CBM is mainly composed of the delocalized In $5s$ orbital.

the result that the V_{Cu} defect has no transition-energy level within the band gap [see Figs. 2(b) and 2(c)]. Meanwhile, the neutral antisite Cu_{In} acceptor defects cannot lead to a deep-level state, since the dangling-bond state coming from the unsaturated Cu $3d$-t_{2g}/S $3p$ antibonding orbital will be located around the VBM. The highly ionized Cu_{In} defect tends to separate the connected Cu_{In} ion and S ion due to the occupied defect state with antibonding character. However, statistics on bond lengths show only minor variations (<0.02 Å) in the lengths of $S - Cu_{In}^0$, $S - Cu_{In}^-$ and $S - Cu_{In}^{2-}$ bonds. This suggests that the primary factor contributing to the total energy increase in the system with a highly charged Cu_{In} defect is the upward movement of the occupied defect state in energy, rather than atomic relaxation, as evidenced by the transition-energy level $\varepsilon(-/2-)$ of the Cu_{In} defect within the band gap [see Figs. 2(b) and 2(c)]. In comparison, the CBM arises from the antibonding state of the In $5s$/S $3p$ orbitals and is dominated by the In $5s$ orbital. As a result of the delocalized spherical shape of the In $5s$ orbital in real space, the conduction-band edge exhibits a pronounced downward bending in reciprocal space, which favors the shallow donor-defect state that is generally derived from the conduction band of the host [58], resembling band-dispersive and defect-tolerant topological materials [59], perovskites [60], and spinel semiconductors [61]. This is corroborated by the result that the dominant In_{Cu} and Cu_i donor defects do not have a defect level in the band gap [see Figs. 2(b) and 2(c)]. Nevertheless, the conduction-band edge can be highly susceptible to the In_{Cu} donor defect because of its significant dispersion and the predominant contribution of the delocalized In $5s$ orbital. The influence of the In_{Cu} defect state on the band-edge fluctuation is discussed below.

Figures 4(a) and 4(b) show the band structures and atomic orbital interaction diagrams of CIS with In_{Cu}^0 and In_{Cu}^{2+} defects. It is seen that the defect states arising from the antibonding state of In_{Cu} $5s$/S $3p$ orbital coupling are located in the conduction band, leading to a downward shift of the conduction-band edge. The band-edge fluctuations of CIS with varying charge states of the In_{Cu} defects are depicted in Fig. S4 within the Supplemental Material [5]. Given the band-tail states and the compensation effects of the In_{Cu} defects, related defects in CIS need to be improved in particular. Recently, P doping was theoretically proposed to heal the deep-level states and band-edge fluctuations resulting from Sn_{Zn} defects by forming a benign $2P_S + Sn_{Zn}$ defect complex in kesterite, Cu_2ZnSnS_4 [21]. In this work, P incorporation is explored to improve the In_{Cu}-related defects in CIS by forming an isoelectronic $2P_S + In_{Cu}$ defect complex. The band structure of CIS with the $2P_S + In_{Cu}$ defect complex [Fig. 4(c)] indicates that the substantial atomic orbital coupling of In_{Cu} σ^*/$2P_S$ $3p$ leads to entry of the antibonding state into the deep conduction band, thereby healing the conduction-band-edge fluctuation, as shown by the similar band-edge topography to that of pristine CIS [see the top and middle panels of Fig. 4(c)]. Additionally, the two residual electrons of the In_{Cu} donor defect are captured by the two P_S defects and accommodated at the two bonding states of

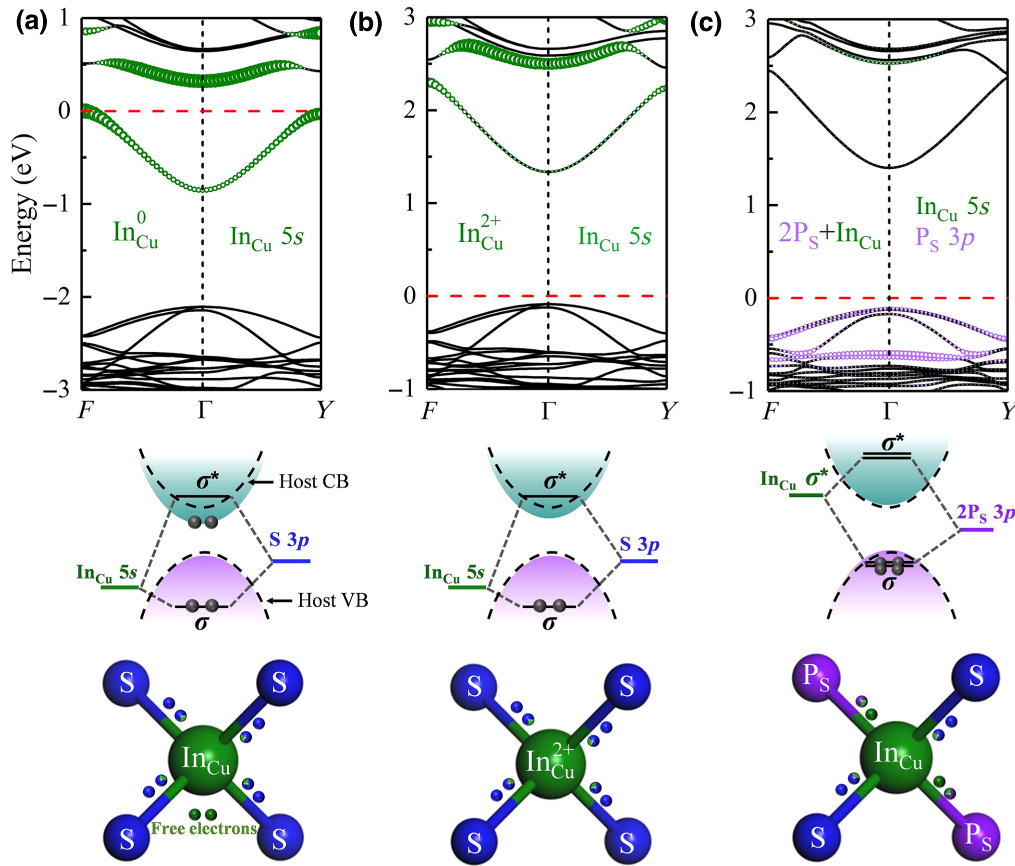

FIG. 4. Band structures, schematic diagrams of atomic orbital interactions, and atomic structures of CIS with defects. Top panel presents band structures weighted by atomic orbitals of related defects, which are represented by colored circles. Red dashed line indicates the highest occupied energy level for electrons. Middle panel illustrates the atomic orbital coupling of defects, the atomic structures of which are displayed in the bottom panel. Cyan and purple parabolas sketch the CB and VB of CIS with defects, respectively, the positions of which relative to those of pristine CIS denoted by black dashed parabolas are determined by the band-edge fluctuations shown in Fig. S4 within the Supplemental Material [5] and Fig. 5(b). (a) In^0_{Cu} and (b) In^{2+}_{Cu} defect systems. CBMs of In^0_{Cu} and In^{2+}_{Cu} systems with and without electron occupation, respectively, are pushed downwards by the antibonding state (σ^*) of In_{Cu} 5*s*/S 3*p* entering the CB, in comparison with the CBM of pristine CIS. (c) $2P_S + In_{Cu}$ defect-complex system. Band-edge fluctuation is healed owing to the orbital coupling of In_{Cu} $\sigma^*/2P_S$ 3*p*, the antibonding and bonding states of which are located in the deep CB and VB, respectively.

In_{Cu} $\sigma^*/2P_S$ 3*p* below the VBM, as schematically illustrated by the middle panel of Fig. 4(c), hence making the system maintain its semiconductor characteristics by satisfying the octet electron-counting rule. Therefore, the possible formation of the $2P_S + In_{Cu}$ defect complex could eliminate the band-tail state induced by the isolated In_{Cu} donor defect and facilitate the desired *p*-type characteristic by consuming its residual electrons at the conduction band.

D. Formation energies and band-edge fluctuations of defect complexes

To promote the formation of the desired $2P_S + In_{Cu}$ defect complex, the formation energies of neutral defect complexes related to P_S and In_{Cu} defects are investigated under varying elemental chemical potentials, as shown in Fig. 5(a). It is seen that the $2P_S + In_{Cu}$ defect complex has the lowest formation energy among these defect complexes under the conditions represented by points *E* ($\mu_{Cu}=-0.14$ eV, $\mu_{In}=0$ eV, $\mu_S=-0.98$ eV, and $\mu_P=-0.06$ eV) and *G* ($\mu_{Cu}=-0.49$ eV, $\mu_{In}=0$ eV, $\mu_S=-0.81$ eV, and $\mu_P=0$ eV), corresponding to the In-rich, S-poor, and P-rich conditions that promote the formation of P_S and In_{Cu} point defects. To facilitate experimental implementation, the region of elemental chemical potential dominated by the expected $2P_S + In_{Cu}$ defect complex is extracted from the phase diagram of CIS and highlighted in gold, as shown in Fig. 2(a), which is undoubtedly located in the In-rich, S-poor, and P-rich region. In addition, this desired chemical potential region avoids the Cu-rich conditions, which eliminate the need for the etching process during experiments and is thus helpful at reducing interfacial

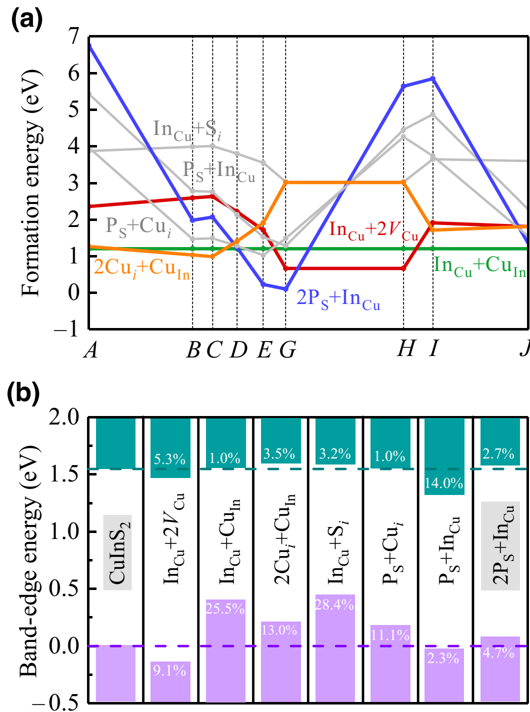

FIG. 5. Formation energies of defect complexes and band-edge fluctuations of CIS influenced by defect complexes. (a) Formation energies of In_{Cu}- and P_S-related isoelectronic defect complexes as functions of elemental chemical potentials with the maximum allowed P-doping amount. Elemental chemical potentials at points *A-B-C-D-E-G-H-I-J* are listed in Table S2 within the Supplemental Material [5], corresponding to the extreme synthesis conditions in the CIS phase diagram in Fig. 2(a). Defect complexes with relatively high and low formation energies are represented by gray lines and colored lines, respectively. (b) Band-edge fluctuations of CIS influenced by defect complexes, referenced to the band-edge position of defect-free CIS. Band-edge energies are aligned by the core level of the 1*s* orbital of the S atoms far away from the defect sites, and the VBM energy of CIS as a reference is set to zero. Percentages marked at the CBM and VBM represent the relative deviations of the band-edge energies from that of pristine CIS. Incorporation of P forming the beneficial $2P_S + In_{Cu}$ defect complex successfully eliminates the band-tail states arising from In_{Cu}-related defects.

recombination at the contact with the CdS buffer layer by presenting a less-defective surface of the CIS absorber [13,14]. The relatively small golden region suggests that the synthesis conditions for the highly efficient CIS solar cell should be carefully controlled.

Band-tail states induced by defect complexes usually increase the probability of carrier recombination, thereby aggravating the loss of V_{OC} in solar cells [62,63]. Without external elemental doping, the desired *p*-type characteristic of CIS is synthesized under S-rich and In-poor conditions, such as point *A* in Fig. 2(a). These conditions facilitate the formation of Cu_{In} acceptor and Cu_i donor point defects, as well as the stubborn In_{Cu} point defect, as shown in Fig. 2(b). Subsequently, neutral $2Cu_i + Cu_{In}$ and $In_{Cu} + Cu_{In}$ defect complexes are also promoted under the synthesis conditions of point *A*, as shown in Fig. 5(a), which significantly raise the VBM [see Fig. 5(b)] due to the upward repulsion of the antibonding state of the strong Cu 3*d*/S 3*p* orbital coupling [34]. In addition, the defect level within the band gap caused by Cu_{In} defect still exists in its related defect complexes, because the cation point defects of defect complexes, connected with the S anion, have only spatial charge transfer and no substantial atomic orbital coupling, as demonstrated by the defect complexes in Cu_2ZnSnS_4 [21]. Given the high formation energies of $In_{Cu} + S_i$, $P_S + Cu_i$, and $P_S + In_{Cu}$ defect complexes, their effects on the band edge of CIS are negligible. These results suggest that pristine CIS encounters severe band-tail states originating from In_{Cu}- and Cu_{In}-related defects.

Owing to the substantial atomic orbital coupling between In_{Cu} σ^* and $2P_S$ 3*p*, as discussed in Sec. III C, the $2P_S + In_{Cu}$ defect complex reduces the band-tail states caused by the stubborn In_{Cu} donor defect, as shown in Fig. 5(b). Moreover, the required In-rich, S-poor, and P-rich conditions [around points *E* and *G* in Fig. 5(a)], promoting the predominant formation of the beneficial $2P_S + In_{Cu}$ defect complex, considerably suppress the formation of harmful Cu_{In} point defects [see Fig. 2(c)] and related $2Cu_i + Cu_{In}$ and $In_{Cu} + Cu_{In}$ defect complexes [see Fig. 5(a)], hence effectively alleviating the defect state within the band gap and band-tail state. In addition, an $In_{Cu} + 2V_{Cu}$ defect complex causes a downward shift in the VBM, as shown in Fig. 5(b), arising from the weakened Cu 3*d*/S 3*p* coupling, which is suppressed due to its high formation energy relative to that of the $2P_S + In_{Cu}$ defect complex under the synthesis conditions around points *E* and *G* in Fig. 5(a). Therefore, the effective formation of the $2P_S + In_{Cu}$ defect complex eventually improves the electrical properties of CIS by relieving the band-tail states and defect states within the band gap.

E. Carrier concentration

Given the strong compensation effect of defects illustrated by the calculation of the defect-formation energy [see Figs. 2(b) and 2(c)], it is difficult to maintain a sufficient *p*-type conductivity as the elemental chemical potential changes. The hole-concentration calculations [see Fig. 6(a)] demonstrate that the *p*-type characteristic of pristine CIS can be achieved with a hole concentration of about 10^{10} cm^{-3} under In-poor and S-rich conditions. The calculated highest hole concentration of pristine CIS is lower than that in experiments (10^{17} cm^{-3}) [12,23], because the real growth process of the chalcopyrite absorber always deviates from the thermodynamic equilibrium conditions adopted in our calculations (see Part V of the Supplemental Material [5] for detailed calculations of the carrier

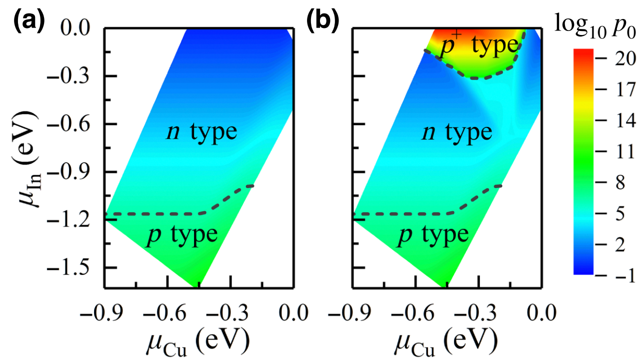

FIG. 6. Contour plot of hole concentration as a function of the chemical potentials of μ_{Cu} and μ_{In} for CIS without P incorporation (a) and with P incorporation (b) under the maximum allowed chemical potential of μ_P. Dashed lines determined by a Fermi level of 0.77 eV located at the midgap separate the regions of *n*-type and *p*-type characteristics. Corresponding Fermi-level contour plot as a function of chemical potentials of μ_{Cu} and μ_{In} is presented in Fig. S5 within the Supplemental Material [5].

concentration [64–66]). On the other hand, the In-rich conditions needed for suppression of the harmful Cu_{In} defects result in an undesired *n*-type conversion. By comparing Figs. 6(a) and 6(b), it is evident that P incorporation has little effect on the intrinsic *p*-type region corresponding to In-poor and S-rich conditions due to the very high formation energy of the $2P_S + In_{Cu}$ defect complex, as shown in Fig. 5(a). Under In-rich, S-poor, and P-rich conditions, P can be efficiently incorporated by forming the energetically favorable neutral $2P_S + In_{Cu}$ defect complex, which consumes the residual electrons of the In_{Cu} defects and yields a high hole concentration in the range of 10^{11}–10^{20} cm^{-3}, as shown in Fig. 6(b), which is in good agreement with previous calculations [24]. Therefore, the formation of the $2P_S + In_{Cu}$ defect complex substantially enhances the *p*-type characteristic of CIS through effective P incorporation under synthesis conditions that can suppress harmful Cu_{In} defects.

IV. CONCLUSIONS

We reveal the origins of the long-stagnated efficiency of pure disulfide CIS in terms of bulk defects, including the restrained *p*-type conductivity resulting from the strong compensation effect of intrinsic defects, the serious band-tail states arising from In_{Cu}- and Cu_{In}-related defects, and the defect states within the band gap induced by the Cu_{In} defect. The isoelectronic $2P_S + In_{Cu}$ defect complex formed by P incorporation can effectively enhance the *p*-type characteristic of CIS by consuming the residual electrons from In_{Cu}-donor defects and alleviate the severe band-tail states by healing the In_{Cu}-related defects, without introducing extra adverse effects. Moreover, the Cu_{In} defects with a defect level within the band gap are successfully suppressed under the In-rich, S-poor, and P-rich conditions required for promoting the formation of the beneficial $2P_S + In_{Cu}$ defect complex, which avoid the Cu-rich conditions, and are thus helpful for achieving a benign absorber surface [13,14]. This study not only elucidates the origins of the inferior photovoltaic performance of CIS but also proposes a feasible way to make the improved bulk defects compatible with the reduction of interfacial recombination. Moreover, an understanding of eliminating the adverse effects of intrinsic defects by defect-complex engineering provides guidance for improving the electrical properties of multicomponent semiconductors.

ACKNOWLEDGMENTS

This research is supported by the National Nature Science Foundation of China (Grants No. 12274114 and No. 12004100), and Key Scientific Research Foundation for Universities of Henan Province (Grant No. 21A140006). We thank the National Supercomputing Center in Zhengzhou for support in performing calculations.

[1] K. Siemer, J. Klaer, I. Luck, J. Bruns, R. Klenk, and D. Bräunig, Efficient $CuInS_2$ solar cells from a rapid thermal process (RTP), Sol. Energy Mater. Sol. Cells **67**, 159 (2001).

[2] H. Hiroi, Y. Iwata, S. Adachi, H. Sugimoto, and A. Yamada, New world-record efficiency for pure-sulfide $Cu(In, Ga)S_2$ thin-film solar cell with Cd-free buffer layer via KCN-free process, IEEE J. Photovoltaics **6**, 760 (2016).

[3] T. Feurer, R. Carron, G. Torres Sevilla, F. Fu, S. Pisoni, Y. E. Romanyuk, S. Buecheler, and A. N. Tiwari, Efficiency improvement of near-stoichiometric $CuInSe_2$ solar cells for application in tandem devices, Adv. Energy Mater. **9**, 1901428 (2019).

[4] M. Nakamura, K. Yamaguchi, Y. Kimoto, Y. Yasaki, T. Kato, and H. Sugimoto, Cd-free $Cu(In, Ga)(Se, S)_2$ thin-film solar cell with record efficiency of 23.35%, IEEE J. Photovoltaics **9**, 1863 (2019).

[5] See the Supplemental Material at http://link.aps.org/supplemental/10.1103/PhysRevApplied.19.064036 for a comparison of the photovoltaic performance of chalcopyrite, the chemical potential conditions for the $CuInS_2$ phase, testing of the supercell size, band-edge fluctuations, and calculation details of the Fermi level and carrier concentration.

[6] P. Würfel and U. Würfel, *Physics of solar cells: From basic principles to advanced concepts* (Wiley-VCH Verlag GmbH & Co. KGaA, Weinheim, Germany, 2016).

[7] M. Turcu, O. Pakma, and U. Rau, Interdependence of absorber composition and recombination mechanism in $Cu(In, Ga)(Se, S)_2$ heterojunction solar cells, Appl. Phys. Lett. **80**, 2598 (2002).

[8] M. Kemell, M. Ritala, and M. Leskelä, Thin film deposition methods for $CuInSe_2$ solar cells, Crit. Rev. Solid State **30**, 1 (2005).

[9] V. Deprédurand, D. Tanaka, Y. Aida, M. Carlberg, N. Fèvre, and S. Siebentritt, Current loss due to recombination in Cu-rich $CuInSe_2$ solar cells, J. Appl. Phys. **115**, 044503 (2014).

[10] A. Lomuscio, T. Rödel, T. Schwarz, B. Gault, M. Melchiorre, D. Raabe, and S. Siebentritt, Quasi-Fermi-level splitting of Cu-poor and Cu-rich $CuInS_2$ absorber layers, Phys. Rev. Appl. **11**, 054052 (2019).

[11] S. Siebentritt, L. Gütay, D. Regesch, Y. Aida, and V. Deprédurand, Why do we make $Cu(In, Ga)Se_2$ solar cells non-stoichiometric?, Sol. Energy Mater. Sol. Cells **119**, 18 (2013).

[12] S. Shukla, M. Sood, D. Adeleye, S. Peedle, G. Kusch, D. Dahliah, M. Melchiorre, G.-M. Rignanese, G. Hautier, R. Oliver, and S. Siebentritt, Over 15% efficient wide-band-gap $Cu(In, Ga)S_2$ solar cell: Suppressing bulk and interface recombination through composition engineering, Joule **5**, 1816 (2021).

[13] H. Elanzeery, M. Melchiorre, M. Sood, F. Babbe, F. Werner, G. Brammertz, and S. Siebentritt, Challenge in Cu-rich $CuInSe_2$ thin film solar cells: Defect caused by etching, Phys. Rev. Mater. **3**, 055403 (2019).

[14] M. Sood, A. Urbaniak, C. Kameni Boumenou, T. P. Weiss, H. Elanzeery, F. Babbe, F. Werner, M. Melchiorre, and S. Siebentritt, Near surface defects: Cause of deficit between internal and external open-circuit voltage in solar cells, Prog. Photovoltaics **30**, 263 (2022).

[15] S. Yu, B. Li, J. Jiang, X. Liu, S. Hao, S. Han, W. Yan, and H. Xin, Solution-processed chalcopyrite solar cells: The grain growth mechanism and the effects of Cu/In mole ratio, Adv. Energy Mater. **12**, 2103644 (2022).

[16] L. Gütay, D. Regesch, J. K. Larsen, Y. Aida, V. Depredurand, A. Redinger, S. Caneva, S. Schorr, C. Stephan, J. Vidal, S. Botti, and S. Siebentritt, Feedback mechanism for the stability of the band gap of $CuInSe_2$, Phys. Rev. B **86**, 045216 (2012).

[17] A. Thomere, C. Guillot-Deudon, M. T. Caldes, R. Bodeux, N. Barreau, S. Jobic, and A. Lafond, Chemical crystallographic investigation on Cu_2S-In_2S_2-Ga_2S_2 ternary system, Thin Solid Films **665**, 46 (2018).

[18] H. Chen, C.-Y. Wang, J.-T. Wang, X.-P. Hu, and S.-X. Zhou, First-principles study of point defects in solar cell semiconductor $CuInS_2$, J. Appl. Phys. **112**, 084513 (2012).

[19] P. Yang, L.-J. Shi, J.-M. Zhang, G.-B. Liu, S. A. Yang, W. Guo, and Y. Yao, Tuning to the band gap by complex defects engineering: Insights from hybrid functional calculations in $CuInS_2$, J. Phys. D: Appl. Phys. **51**, 025105 (2018).

[20] J. J. Frick, G. Cheng, S. Kushwaha, N. Yao, S. Wagner, A. B. Bocarsly, and R. J. Cava, Observation of $[V_{Cu}{}^{1-}In_i{}^{2+}V_{Cu}{}^{1-}]$ defect triplets in Cu-deficient $CuInS_2$, J. Phys. Chem. C **124**, 26415 (2020).

[21] K. Zhao, H. Xiang, R. Zhu, C. Liu, and Y. Jia, Passivation principle of deep-level defects: A study of Sn_{Zn} defects in kesterites for high-efficient solar cells, J. Mater. Chem. A **10**, 2849 (2022).

[22] J. M. Burst, J. N. Duenow, D. S. Albin, E. Colegrove, M. O. Reese, J. A. Aguiar, C.-S. Jiang, M. Patel, M. M. Al-Jassim, D. Kuciauskas, *et al.*, CdTe solar cells with open-circuit voltage breaking the 1 V barrier, Nat. Energy **1**, 16015 (2016).

[23] T. Kato, H. Yamaguchi, T. Nakamura, Y. Nabetani, and T. Matsumoto, Incorporation of P in $CuInS_2$ using InP as a p-type dopant, Phys. Status Solidi C **3**, 2606 (2006).

[24] T. Yamamoto and H. Katayama-Yoshida, Control of valence states by a codoping method in $CuInS_2$, Sol. Energy Mater. Sol. Cells **49**, 391 (1997).

[25] G. Kresse and J. Furthmüller, Efficiency of *ab-initio* total energy calculations for metals and semiconductors using a plane-wave basis set, Comput. Mater. Sci. **6**, 15 (1996).

[26] G. Kresse and J. Furthmüller, Efficient iterative schemes for *ab initio* total-energy calculations using a plane-wave basis set, Phys. Rev. B **54**, 11169 (1996).

[27] G. Kresse and D. Joubert, From ultrasoft pseudopotentials to the projector augmented-wave method, Phys. Rev. B **59**, 1758 (1999).

[28] J. P. Perdew, K. Burke, and M. Ernzerhof, Generalized Gradient Approximation Made Simple, Phys. Rev. Lett. **77**, 3865 (1996).

[29] J. Heyd, G. E. Scuseria, and M. Ernzerhof, Hybrid functionals based on a screened coulomb potential, J. Chem. Phys. **118**, 8207 (2003).

[30] M. V. Yakushev, A. V. Mudryi, I. V. Victorov, J. Krustok, and E. Mellikov, Energy of excitons in $CuInS_2$ single crystals, Appl. Phys. Lett. **88**, 011922 (2006).

[31] H. J. Monkhorst and J. D. Pack, Special points for brillouin-zone integrations, Phys. Rev. B **13**, 5188 (1976).

[32] S.-H. Wei and S. B. Zhang, Defect properties of $CuInSe_2$ and $CuGaSe_2$, J. Phys. Chem. Solids **66**, 1994 (2005).

[33] B. Tell, J. L. Shay, and H. M. Kasper, Electrical properties, optical properties, and band structure of $CuGaS_2$ and $CuInS_2$, Phys. Rev. B **4**, 2463 (1971).

[34] S. B. Zhang, S.-H. Wei, and A. Zunger, Defect physics of the $CuInSe_2$ chalcopyrite semiconductor, Phys. Rev. B **57**, 9642 (1998).

[35] A. Zunger and S.-H. Wei, in *AIP Conference Proceedings*, (American Institute of Physics, Lakewood, Colorado (USA), 1996), Vol. 353, pp. 155–160.

[36] Y.-J. Zhao and A. Zunger, Electronic structure and ferromagnetism of Mn-substituted $CuAlS_2$, $CuGaS_2$, $CuInS_2$, $CuGaSe_2$, and $CuGaTe_2$, Phys. Rev. B **69**, 104422 (2004).

[37] J. E. Jaffe and A. Zunger, Theory of the band-gap anomaly in ABC_2 chalcopyrite semiconductors, Phys. Rev. B **29**, 1882 (1984).

[38] Z.-K. Yuan, S. Chen, H. Xiang, X.-G. Gong, A. Walsh, J.-S. Park, I. Repins, and S.-H. Wei, Engineering solar cell absorbers by exploring the band alignment and defect disparity: The case of Cu- and Ag-based kesterite compounds, Adv. Funct. Mater. **25**, 6733 (2015).

[39] S. B. Zhang, S.-H. Wei, and A. Zunger, Microscopic Origin of the Phenomenological Equilibrium "Doping Limit Rule" in n-Type III-V Semiconductors, Phys. Rev. Lett. **84**, 1232 (2000).

[40] C. H. Henry, Limiting efficiencies of ideal single and multiple energy gap terrestrial solar cells, J. Appl. Phys. **51**, 4494 (1980).

[41] A. Klein, T. Löher, Y. Tomm, C. Pettenkofer, and W. Jaegermann, Band lineup between CdS and ultra high

vacuum-cleaved $CuInS_2$ single crystals, Appl. Phys. Lett. **70**, 1299 (1997).

[42] Y. Hashimoto, K. Takeuchi, and K. Ito, Band alignment at $CdS/CuInS_2$ heterojunction, Appl. Phys. Lett. **67**, 980 (1995).

[43] L. Weinhardt, O. Fuchs, D. Groß, G. Storch, E. Umbach, N. G. Dhere, A. A. Kadam, S. S. Kulkarni, and C. Heske, Band alignment at the $CdS/Cu(In, Ga)S_2$ interface in thin-film solar cells, Appl. Phys. Lett. **86**, 062109 (2005).

[44] B. Johnson, L. Korte, T. Lußky, J. Klaer, and I. Lauermann, $CuInS_2$-CdS heterojunction valence band offset measured with near-UV constant final state yield spectroscopy, J. Appl. Phys. **106**, 073712 (2009).

[45] A. Klein, Energy band alignment in chalcogenide thin film solar cells from photoelectron spectroscopy, J. Phys.: Condens. Matter **27**, 134201 (2015).

[46] R. Scheer, Open questions after 20 years of $CuInS_2$ research, Prog. Photovoltaics **20**, 507 (2012).

[47] T. Dullweber, G. Hanna, W. Shams-Kolahi, A. Schwartzlander, M. A. Contreras, R. Noufi, and H. W. Schock, Study of the effect of gallium grading in $Cu(In, Ga)Se_2$, Thin Solid Films **361–362**, 478 (2000).

[48] S.-H. Wei, S. B. Zhang, and A. Zunger, Effects of Ga addition to $CuInSe_2$ on its electronic, structural, and defect properties, Appl. Phys. Lett. **72**, 3199 (1998).

[49] T. Minemoto, T. Matsui, H. Takakura, Y. Hamakawa, T. Negami, Y. Hashimoto, T. Uenoyama, and M. Kitagawa, Theoretical analysis of the effect of conduction band offset of window/CIS layers on performance of CIS solar cells using device simulation, Sol. Energy Mater. Sol. Cells **67**, 83 (2001).

[50] S.-H. Wei, Overcoming the doping bottleneck in semiconductors, Comp. Mater. Sci. **30**, 337 (2004).

[51] S. B. Zhang and J. Northrup, Chemical Potential Dependence of Defect Formation Energies in GaAs: Application to Ga Self-Diffusion, Phys. Rev. Lett. **67**, 2339 (1991).

[52] D. R. Lide, *CRC handbook of chemistry and physics* (CRC press, Boca Raton, Florida, 2004), Vol. 85.

[53] C. Freysoldt, J. Neugebauer, and C. G. Van de Walle, Electrostatic interactions between charged defects in supercells: Electrostatic interactions between charged defects in supercells, Phys. Status Solidi B **248**, 1067 (2011).

[54] C. Freysoldt, J. Neugebauer, and C. G. Van de Walle, Fully *Ab Initio* Finite-Size Corrections for Charged-Defect Supercell Calculations, Phys. Rev. Lett. **102**, 016402 (2009).

[55] C. Freysoldt, SXDEFECTALIGN, http://www.sphinxlib.de

[56] J. Binsma, L. Giling, and J. Bloem, Luminescence of $CuInS_2$: I. The broad band emission and its dependence on the defect chemistry, J. Lumin. **27**, 35 (1982).

[57] J. E. Jaffe and A. Zunger, Electronic structure of the ternary chalcopyrite semiconductors $CuAlS_2$, $CuGaS_2$, $CuInS_2$, $CuAlSe_2$, $CuGaSe_2$, and $CuInSe_2$, Phys. Rev. B **28**, 5822 (1983).

[58] S.-H. Wei and S. B. Zhang, Chemical trends of defect formation and doping limit in II-VI semiconductors: The case of CdTe, Phys. Rev. B **66**, 155211 (2002).

[59] M. Huang, S. Wang, T. Zhang, and S. Chen, Searching for band-dispersive and defect-tolerant semiconductors from element substitution in topological materials, J. Am. Chem. Soc. **144**, 4685 (2022).

[60] W.-J. Yin, T. Shi, and Y. Yan, Unusual defect physics in $CH_3NH_3PbI_3$ perovskite solar cell absorber, Appl. Phys. Lett. **104**, 063903 (2014).

[61] H. Liang, H. Xiang, R. Zhu, C. Liu, and Y. Jia, The structural stability and defect-tolerance of ionic spinel semiconductors for high-efficiency solar bells, J. Mater. Chem. A **9**, 14566 (2021).

[62] M. Nishiwaki, K. Nagaya, M. Kato, S. Fujimoto, H. Tampo, T. Miyadera, M. Chikamatsu, H. Shibata, and H. Fujiwara, Tail state formation in solar cell materials: First principles analyses of zincblende, chalcopyrite, kesterite, and hybrid perovskite crystals, Phys. Rev. Mater. **2**, 085404 (2018).

[63] M. J. Romero, H. Du, G. Teeter, Y. Yan, and M. M. Al-Jassim, Comparative study of the luminescence and intrinsic point defects in the kesterite Cu_2ZnSnS_4 and chalcopyrite $Cu(In, Ga)Se_2$ thin films used in photovoltaic applications, Phys. Rev. B **84**, 165324 (2011).

[64] S. Chen, A. Walsh, X.-G. Gong, and S.-H. Wei, Classification of lattice defects in the kesterite Cu_2ZnSnS_4 and $Cu_2ZnSnSe_4$ earth-abundant solar cell absorbers, Adv. Mater. **25**, 1522 (2013).

[65] J. S. Park, S. Kim, Z. Xie, and A. Walsh, Point defect engineering in thin-film solar cells, Nat. Rev. Mater. **3**, 194 (2018).

[66] K. Seeger, *Semiconductor physics* (Springer-Verlag, Berlin, Heidelberg, 2013).